Available online at www.sciencedirect.com

SciVerse ScienceDirect

Physics Procedia 39 (2012) 717 – 725

Physics Procedia

LANE 2012

Ultra-fast movies resolve ultra-short pulse laser ablation and bump formation on thin molybdenum films

Matthias Domke*, Stephan Rapp, Heinz Huber

Munich University of Applied Sciences, Lothstrasse 34, 80335 Munich, Germany

Abstract

For the monolithic serial interconnection of CIS thin film solar cells, 470 nm molybdenum films on glass substrates must be separated galvanically. The single pulse ablation with a 660 fs laser at a wavelength of 1053 nm is investigated in a fluence regime from 0.5 to 5.0 J/cm². At fluences above 2.0 J/cm² bump and jet formation can be observed that could be used for creating microstructures. For the investigation of the underlying mechanisms of the laser ablation process itself as well as of the bump or jet formation, pump probe microscopy is utilized to resolve the transient ablation behavior.

Keywords: ultra-short pulse; laser ablation; thin film; molybdenum; pump-probe; microbump; nanojet

1. Introduction

About 500 nm thin molybdenum films on glass substrates serve as the p-contact of CIS (Copper-Indium-Diselenide) thin-film solar cells. These films must be galvanically separated in about 5 mm wide stripes for the monolithic serial interconnection of the CIS cells [1-5]. First results of layer and glass-substrate side scribing of thin molybdenum layers using ns-pulses were published in 2000 [3]. In both cases, nanosecond pulses create pronounced thermal effects, such as burrs and micro cracks, in the remaining molybdenum layer and in the underlying glass substrate [3, 6]. Nevertheless, “Mo-side” ns-laser processes have been established in current production lines [6]. Later, ultra-short laser pulses were applied from the Mo side, enabling selective ablation of the Mo, thereby reducing thermal effects [2, 7]. In contrast, ultra-short pulse laser scribing of Mo films from the glass side, first published by our group in 2009 [8], creates ablated spots and trenches free from thermal effects, with clean and regular edges.

* Corresponding author. Tel.: +49-89-1265-3677 .
E-mail address: matthias.domke@hm.edu .

 doi:10.1016/j.phpro.2012.10.093

If the Mo film is irradiated from the glass substrate side with ultra-short laser pulses, three different fluence regimes F_1 - F_3 can be distinguished as shown in Fig. 1, upper row. At $F_1 > F_{th}$ the Mo film is caused to bulge. The threshold fluence $F_{th} \sim 0.3$ J/cm² for Mo film bulging is almost equal to the ablation threshold of bulk molybdenum, because the bulging is initiated by confined ablation of the Mo film [5, 9, 10]. Thus, both thresholds are named F_{th} in the following. A lift-off of an intact Mo disk is initiated at a fluence $F_2 > 2 \cdot F_{th}$. Glass damage occurs at $F_3 > F_2$, depending on the intensity of the pulse due to non-linear absorption. The transient ablation behavior in these three fluence regimes were already investigated by our group utilizing ultra-fast pump-probe microscopy [10].

Remarkably, the energy per ablated volume for the removal of a Mo disk is about 30 J/mm³, which is below the total evaporation energy of 78 J/mm³ for molybdenum [1]. Moreover, the entire film is selectively removed by a single pulse. Thus, glass side scribing enables high process speeds at low energies. For example, with a 10 W laser system process speeds of up to 20 m/s could be achieved at pulse energies below 10 µJ. In contrast, film side scribing of Mo is performed at fluences F_4 just above the ablation threshold F_{th}, as shown in Fig. 1 lower row, and at high overlap rates [2]. The molybdenum is then completely evaporated by multiple pulses. In this case, the energy per ablated volume is about 260 J/mm³. Consequently, the process speed is reduced by a factor of ten to about 2 m/s with the same 10 W laser system. However, current ultra-short pulse laser systems provide pulse energies of above 100 µJ. Thus, fluences above 16 J/cm² can be achieved, assuming a spot diameter of about 40 µm at the 1/e² intensity level. But if the fluence is increased well above the ablation threshold – in order to remove the entire film with a single pulse – micro cracks, micro bumps and jets, burrs and melt formations are generated (Fig. 1, lower row).

The observed bump and jet formations – which are disadvantageous for laser scribing - can be used to generate various kinds of microstructures. Recent investigations showed that the formation of bumps and jets is a universal effect for laser irradiation of thin metal films from the film side [11]. The form of the created structure depends on the material properties of the metal layer, the layer thicknesses, the spot size and the pulse duration. Bumps and jets were observed for fs-, ps-, and ns-pulse durations [11].

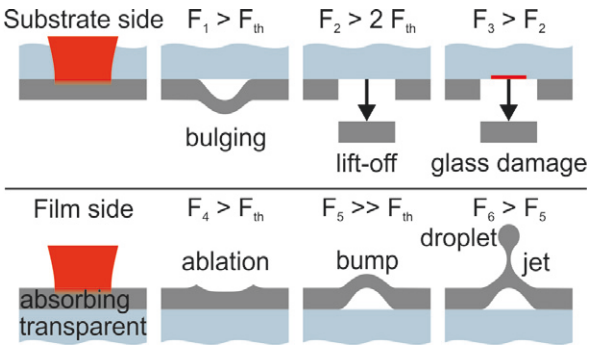

Fig. 1. Resulting structures of substrate side irradiation (upper row) and film side irradiation (lower row) of a thin metal film on a transparent substrate at different fluences. For substrate side irradiation, the metal layer is caused to bulge at a fluence F_1 above the ablation threshold F_{th} of bulk metal. At a fluence F_2, about twice above the ablation threshold F_{th}, an intact Mo disk is lifted off. At higher fluences F_3, the substrate is damaged due to nonlinear absorption. For film side irradiation, a fraction of the molybdenum is ablated at fluences F_4 above the ablation threshold F_{th}. A bump is formed at higher fluences F_5, and at even higher fluences F_6, a jet is formed or a droplet is ejected

Kuznetsov et al. [12] described the process as follows: The laser pulse melts the layer completely. A liquid bump then detaches from the substrate due to relaxation of mechanical stresses. The surface tension restrains the expansion and decelerates the bump. The bump then collapses and two counterjets form in and outside the bump. At higher fluences a droplet is ejected from the top of the jet (Fig. 1, upper row, F3). Recently, Koch et al. [11] published pump-probe microscopy investigations of the bump formation on a 100 nm gold film. The transient behavior of the bump and jet formation was observed from the side with a temporal resolution of 10 ns.

We already used pump-probe microscopy to investigate the fundamental mechanisms of glass side ablation [10, 13-15]. Because of the high temporal dynamic range of the lift-off process - from femtoseconds to microseconds - the setup comprises an ultra-fast pump pulse (660 fs FWHM) combined with an optical delay for the first 4 ns and an electronic delay (600 ps FWHM) for longer delay times [15]. This improved setup now enables investigations of entire laser ablation processes.

In this paper we present for the first time to our knowledge pump-probe investigations of the Mo film ablation in a top view at fluences of 0.5 and 1.5 J/cm², and of a bump and jet formation at 3.0 and 5.0 J/cm². The results reveal the driving mechanisms of Mo film ablation at low fluences and the nature for an upper process window at high fluences. Moreover, the transient behaviour of bump and jet formations, which can be used for creating microstructures, is discussed.

2. Material and Methods

A detailed description of the pump-probe microscopy setup is given in [15]. The paper also describes the calibration of the temporal delay time zero point and aspects of the image processing. A short overview of the setup is shown schematically in Fig. 2. An ultrafast laser source (High Q Laser, model femtoREGEN) emitting 660 fs (FWHM) pulses at a centre wavelength of 1053 nm, is divided into pump- and probe pulse by a beam splitter behind the laser exit (beam splitter 1, Fig. 2). The pump pulse, used for initiating the ablation, is focused by a f = 150 mm lens on the sample, to a spot size of about 40 µm diameter (@ the 1/e² intensity level). The angle of incidence of the pump-pulse is about 35 degrees with respect to the microscope objective axis, which is oriented parallel to the sample surface normal. The probe pulse, used for illuminating the sample, is frequency doubled by a lithium triborate (LBO) crystal to a wavelength of 527 nm with a pulse duration of about 510 fs (FWHM). The probe pulse is directed towards the sample via an optical delay line mounted on a translation stage, which allows delay times of up to 4 ns. For probing at delay times above 4 ns, an actively q-switched 600 ps (FWHM) laser source (AOT, model ACE AOT-YVO-25QSP) operating at a wavelength of 532 nm is used. Both probe pulses are combined in a beam splitter (beam splitter 3, Fig. 2) for coaxial illumination of the sample.

The laser-material interaction region is imaged by a microscope objective (20x magnification, NA = 0.29, and 30.8 mm working distance) and an 8 bit CCD camera. The calculated spatial resolution of the microscopic imaging is about 2 µm. The temporal resolution or minimum instrumental response time of the pump-probe setup can be estimated using the cross correlation width of pump and probe pulse, in this case approximately 840 fs (FWHM), assuming a Gaussian pulse form. Measurements of the background noise of a single shot revealed a pixel reflectivity resolution $\Delta R/R$ of about 2 %, limited by the 8 bit CCD camera used.

For creating a stop-motion movie of the ablation process, successive single pulse ablations are captured at increasing delay times. Thus, the reproducibility of each image depends on the pulse to pulse fluctuations of the pump laser. A standard deviation of 1% was measured.

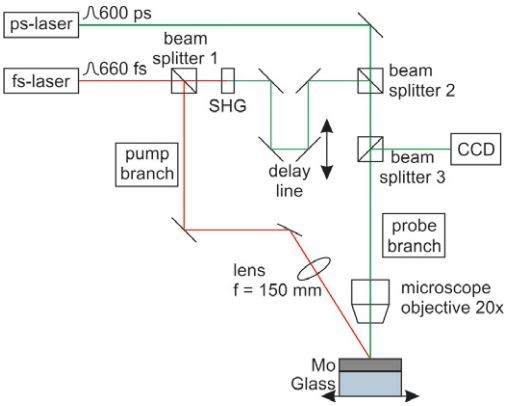

Fig. 2. Pump-probe microscopy setup. The pump-pulse (red branch) is focused on the Mo layer to initiate the ablation. The probe pulse (green branch) illuminates the sample at different delay times that are imaged by a microscope and CCD camera. Up to 4 ns, a frequency doubled 660 fs pulse is delayed on a linear stage. Above 4 ns, a 600 ps probe pulse is triggered by an electronic delay

3. Results and Discussion

Molybdenum films with a thickness of 470 nm on a 3 mm thick glass substrate were irradiated from the Mo side. Fig. 3 shows confocal images (upper row), cross sections (middle row), and microscope images (lower row) of the Mo film after the irradiation at 4 different fluences. At 0.5 J/cm² only a few nm of the Mo film are ablated. At 1.5 J/cm² the ablated region increases. In the confocal microscope images a micro crack crossing the center of the ablated region can be observed. The cross section reveals that the Mo is also elevated by a few 100 nm. At 3.0 J/cm² the Mo film shows a bump formation in the center with a height of about 500 nm – which is about the thickness of the film. At 5.0 J/cm², melting formations of about 1.5 µm height can be observed. Moreover, the Mo film was uncovered inside the bump region.

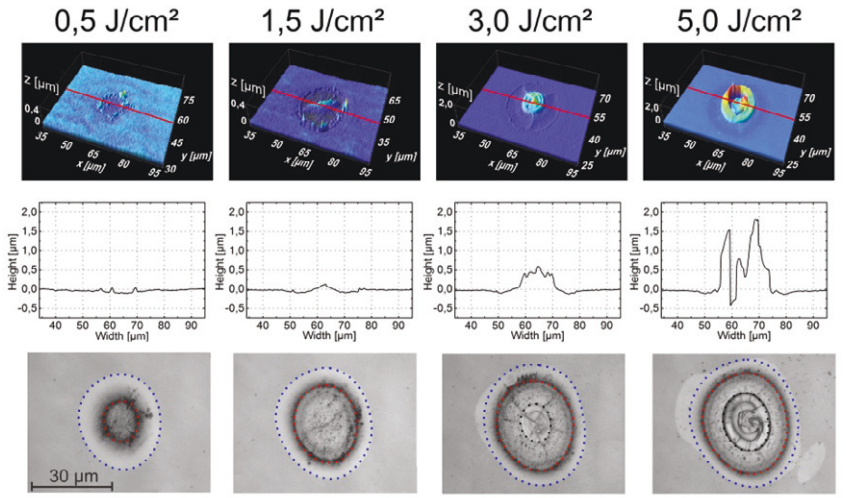

Fig. 3. Confocal microscope images (upper row), cross section of the irradiated area (middle row), and microscope images from the top (lower row) of irradiated Mo films at fluences of 0.5, 1.5, 3.0, and 5.0 J/cm² from left to right. The blue dots in the microsope images (lower row) indicate heat affection, the red dots ablation, and the black dots the bump and jet formation

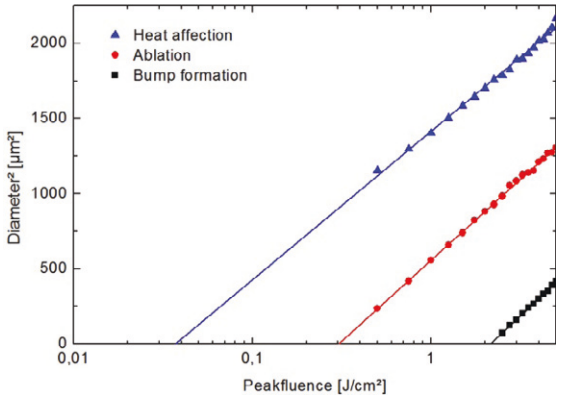

Fig. 4. Diameter squared of the regions of heat affection (blue triangles), ablation (red dots) and bump formation (black squares) versus the applied fluence. The intersection point of the fit curve by the method of Liu [16] with the x-axis defines the threshold for these three regimes. The threshold value for the heat affection is about 0.04 J/cm², for the ablation it is about 0.30 J/cm², and for bump formation it is about 2.15 J/cm²

If a Gaussian laser pulse is used for bulk material ablation, the area of the ablated spot increases linear with the logarithm of the applied fluence. The fluence, where the interpolated diameter is zero is called the ablation threshold [16]. In Fig. 3, three different regions at the irradiated spot can be distinguished that are related to heat affection, ablation and bump formation from the outside to the inside. In Fig. 3, the diameter squared of these regions is plotted against the applied fluence. The threshold value for heat affection is about 0.04 J/cm², for the ablation it is about 0.30 J/cm², and for bump formation it is about 2.15 J/cm².

The columns in Fig. 5 show time-resolved images of Mo side irradiation with fluences of 0.5 J/cm²,1.5 J/cm², 3.0 J/cm², and 5.0 J/cm² from left to right. The image sequences correspond to the confocal and microscope images in Fig. 3. A general transient ablation behavior can be observed for all fluences and will be explained in the next paragraph. The mechanisms of bump and jet formation at 3.0 and 5.0 J/cm² are described in the paragraph afterwards.

The laser pulse is absorbed in the molybdenum within the pulse duration of about 660 fs at delay time zero. Subsequently, the reflectivity in the center slightly increases within 1 ps due to either electron heating [17] or ultrafast melting [18]. Between 10 and 100 ps, the reflectivity in the center decreases as a consequence of probe light scattering and absorption in an expanding two-phase regime, containing gas and liquid [19, 20]. At 1 ns, the reflectivity increases again, due to expansion of highly pressurized material [21]. Moreover, an expanding ring is observed outside the ablated region at 10 and 30 ns. The diameter of the ring increases with time as shown in Fig. 6. At a fluence of 0.5 J/cm² the expansion starts at about 6 ns and for 5.0 J/cm² at 3 ns. An initial velocity can be calculated by the relation $v = \Delta r/(t_2-t_1)$, where r is the radius of the expanding ring and t_1 and t_2 are the first two delay times when the ring is observed. The initial velocities at 0.5 J/cm² and 5.0 J/cm² were calculated to be about 1000 m/s and 4000 m/s, respectively. In other pump-probe investigations, which showed the laser ablation from the side, a shock wave was observed that propagated in air at comparable delay times [21, 22]. Thus, the ring in Fig. 5 is related to a shock wave in air and not a shock wave in the metal film.

At 30 ns and 100 ns, an increasing grainy region can be observed over the ablated spot. At 1 µs the entire image appears grainy. The nature of the grainy structure could be the ejection of small particles that cause light scattering. Because the particles cannot be resolved individually, their size must be smaller

than 2 µm, which is the spatial resolution of the microscope. At 10 µs the final state of the ablation process is reached.

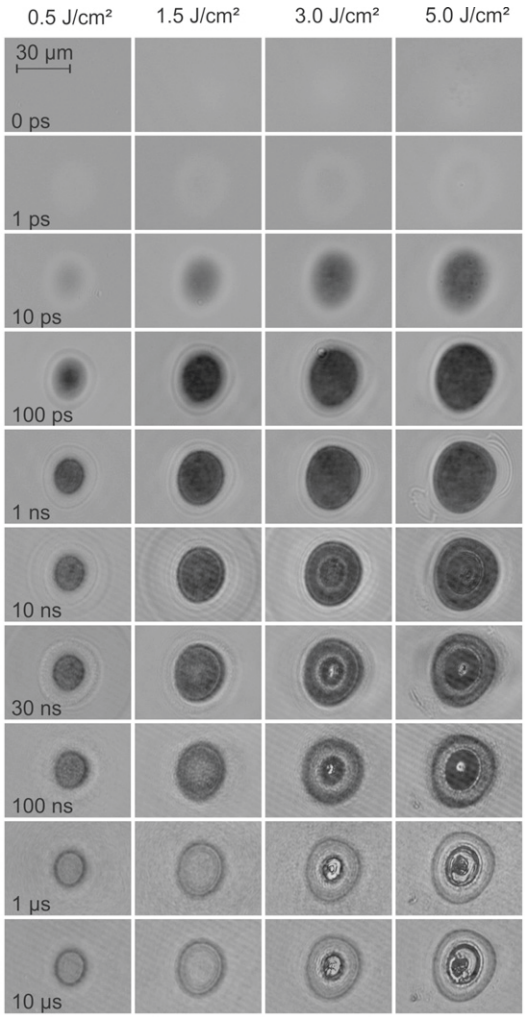

Fig. 5. Pump-probe microscopy images of Mo side irradiation with fluences of 0.5, 1.5, 3.0, and 5.0 J/cm² from the left to right column. The delay times for each row are shown in the left columns and apply to all columns

At 3.0 J/cm² and 5.0 J/cm² the temporal behavior of bump and jet formation can be observed. At 10 ns, a bright ring occurs inside the black region at both fluences, which could be related to the onset of bump formation for two reasons. First, the diameter of the bright ring corresponds to the bump region. Second, the bump formation on gold films starts at around 10 ns, as shown by Koch et al. [11]. At 30 and 100 ns, a bright dot in the center can be observed in Fig. 5. This observation could be related to a jet or droplet formation, which would be in good agreement with the observations of Koch et al. [11], who showed that a jet leaves the bump at about 50 ns. In comparable pump-probe microscopy investigation, Willis et al. [23] related bright regions to low surface tension and dark regions to high surface tension. The displacement of material was explained by surface-tension-driven flow, moving from low to high surface

tension regions. Adopting this theory, the bright ring inside the black region (compare Fig. 5, 10 ns) could be related to a region with low surface tension. Consequently, a surface-tension-driven flow could be directed from the ring to the center, forming a jet, as well as to the edges, building up material.

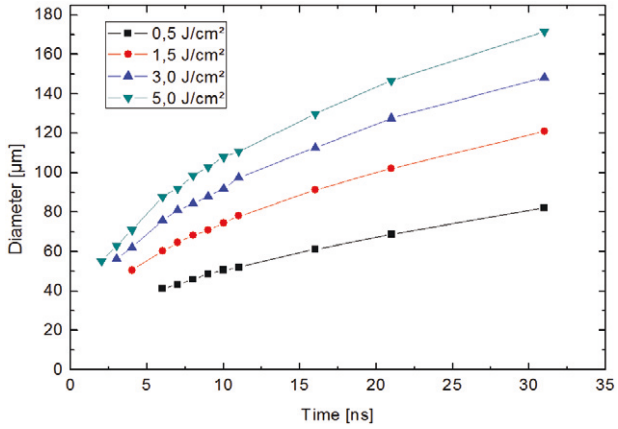

Fig. 6. Diameter of the shock wave front in dependency of time for different fluences. For higher fluences the shock wave expands earlier and with a higher initial velocity. For 0.5 J/cm² the shock wave starts at about 6 ns with an initial velocity of about 1000 m/s. For 5.0 J/cm² the shock wave starts at about 3 ns with an initial velocity of about 4000 m/s

In the final state, which is reached at about 1 to 10 µs, a bump formation on the molybdenum is observed for a fluence of 3.0 J/cm² (Fig 3). In this case, the jet might have collapsed and merged with the bump between 100 ns and 1 µs. At 5.0 J/cm² the confocal image in Fig. 3 shows solidified melting jets and that the glass substrate is partially uncovered. Two scenarios could have caused this structure. In the first scenario, the jet might have ejected a droplet that has fallen into the melt pool and pushed the melting to side. Solidification of the melting could result in the structures observed in Fig. 3. In the second scenario, a droplet could have been ejected and landed somewhere on the Mo surface. The relaxation of the jet might have formed the observed structure.

4. Conclusion

A pump-probe microscopy setup is utilized to record ultrafast stop-motion movies of the laser ablation process of 470 nm thick molybdenum films on glass. The Mo-side was irradiated with a fluence of 0.5, 1.5, 3.0, and 5.0 J/cm².

Observations and measurements show a general ablation behavior for all fluences. After absorbing a 660 fs pump pulse, ultrafast melting is initiated in the molybdenum layer at about 1 ps. At 10 ps, a phase explosion is observed, generating an expanding homogeneous gas-liquid mixture. At a fluence of 0.5 J/cm², a shock wave is injected in air with an initial velocity of 1000 m/s at about 6 ns. At 5.0 J/cm², the shock wave expands with an initial velocity of 4000 m/s at 3 ns. Particle ejections can be observed between 100 ns and 10 µs. At fluences above 2.0 J/cm² bump and jet formations are observed between 30-100 ns. At 3.0 J/cm² the jet collapses and a bump is formed in the final state. At 5.0 J/cm² a droplet is ejected that either leaves a melt formation or falls back into the melt pool and pushes the melt to the side.

The results show that Mo film irradiation at fluences above 2 J/cm² causes bump and jet formation, which could be used for creating microstructures. Thus, a multi-pulse ablation at fluences just above the

ablation threshold of 0.3 J/cm² reduces thermal effects for Mo side scribing. However, glass side scribing should be preferred, because clean and damage free structures can be created at ten times faster process speeds. For example, process speeds of up to 20 m/s could be achieved with a 10 W laser system.

Acknowledgement

This work was partly funded by the German Federal Ministry for the Environment, Nature Conservation and Nuclear Safety within the project 'SECIS', under Grant No. 0325043, and by the German Federal Ministry of Education and Research within the project 'METASOLAR', under Grant No. 02PO2851. We thank AVANCIS GmbH & Co. KG Munich R&D for providing the Mo samples.

References

[1] Heise, G.; Englmaier, M.; Hellwig, C.; Kuznicki, T.; Sarrach, S., Huber, H.P.: Laser ablation of thin molybdenum films on transparent substrates at low fluences. Appl. Phys. A; 2011; 102: pp. 173-178.

[2] Zoppel, S.; Huber, H., Reider, G.A.: Selective ablation of thin Mo and TCO films with femtosecond laser pulses for structuring thin film solar cells. Appl. Phys. A; 2007; 89: pp. 161-163.

[3] Compaan, A.D.; Matulionis, I., Nakade. Laser scribing of polycrystalline thin films. Opt. Laser Eng.; 2000; 34: pp. 15-45.

[4] Heise, G.; Heiss, A.; Hellwig, C.; Kuznicki, T.; Vogt, H.; Palm, J., et al.: Optimization of picosecond laser structuring for the monolithic serial interconnetion of CIS solar cells. Prog. Photovoltaics; 2012: pp.

[5] Heise, G.; Konrad, J.; Sarrach, S.; Sotrop, J., Huber, H.P.: Directly induced ablation of metal thin films by ultrashort laser pulses. Proc. SPIE - Int. Soc. Opt. Eng.; 2011; 7925: 792511.

[6] Huber, H.P.; Herrnberger, F.; Kery, S., Zoppel, S.: Selective structuring of thin-film solar cells by ultrafast laser ablation. Proc. SPIE - Int. Soc. Opt. Eng.; 2008; 6881: 688145.

[7] Hermann, J.; Benfarah, M.; Coustillier, G.; Bruneau, S.; Axente, E.; Guillemoles, J.-F., et al.: Selective ablation of thin films with short and ultrashort laser pulses. Appl. Surf. Sci.; 2006; 252: pp. 4814-4818.

[8] Huber, H.P.; Englmaier, M.; Hellwig, C.; Heiss, A.; Kuznicki, T.; Kemnitzer, M., et al.: High speed structuring of CIS thin-film solar cells with picosecond laser ablation. Proc. SPIE - Int. Soc. Opt. Eng.; 2009; 7203: 720324.

[9] Heise, G.; Domke, M.; Konrad, J.; Sarrach, S.; Sotrop, J., Huber, H.P.: Laser lift-off initiated by direct induced ablation of different metal thin films with ultra short laser pulses. J. Phys. D. App. Phys.; 2012; 45: pp. 315303.

[10] Domke, M.; Rapp, S.; Schmidt, M., Huber, H.P.: Ultra-fast movies of thin-film laser ablation. Appl. Phys. A; 2012; 109: pp. 409-420.

[11] Koch, J.; Unger, C., Chichkov, B.N.: Heat-induced structure formation in metal films generated by single ultrashort laser pulses. 2012; 8244: 824408.

[12] Kuznetsov, A.I.; Unger, C.; Koch, J., Chichkov, B.N.: Laser-induced jet formation and droplet ejection from thin metal films. Appl. Phys. A; 2012; 106: pp. 479-487.

[13] Domke, M.; Heise, G.; Richter, I.; Sarrach, S., Huber, H.P.: Pump-probe investigations on the laser ablation of CIS thin film solar cells. Phys. Procedia; 2011; 12: pp. 399-406.

[14] Domke, M.; Rapp, S.; Heise, G., Huber, H.P.: Time and space resolved microscopy of induced ablation with ultrashort laser pulses. Proc. SPIE - Int. Soc. Opt. Eng.; 2012; 8243: 824308.

[15] Domke, M.; Rapp, S.; Schmidt, M., Huber, H.P.: Ultrafast pump-probe microscopy with high temporal dynamic range. Opt. Express; 2012; 20: pp. 10330-10338.

[16] Liu, J.M.: Simple technique for measurements of pulsed Gaussian-beam spot sizes. Opt. Lett.; 1982; 7: pp. 196-198.

[17] Hohlfeld, J.; Wellershoff, S.-S.; Guedde, J.; Conrad, U.; Jaehnke, V., Matthias, E.: Electron and lattice dynamics following optical excitation of metals. Chem. Phys.; 2000; 251: pp. 237-258.
[18] Rethfeld, B.; Sokolowski-Tinten, K.; Von Der Linde, D., Anisimov, S.I.: Timescales in the response of materials to femtosecond laser excitation. Appl. Phys. A; 2004; 79: pp. 767-769.
[19] Von Der Linde, D.; Sokolowski-Tinten, K., Bialkowski, J.: Laser-solid interaction in the femtosecond time regime. Appl. Surf. Sci.; 1997; 109-110: pp. 1-10.
[20] Von Der Linde, D., Sokolowski-Tinten, K.: Physical mechanisms of short-pulse laser ablation. Appl. Surf. Sci.; 2000; 154: pp. 1-10.
[21] Mingareev, I., Horn, A.: Melt dynamics of aluminum irradiated with ultrafast laser radiation at large intensities. J. Appl. Phys.; 2009; 106: pp. 013513.
[22] Jandeleit, J.; Horn, A.; Weichenhain, R.; Kreutz, E.W., Poprawe, R.: Fundamental investigations of micromachining by nano- and picosecondlaser radiation. Appl. Surf. Sci.; 1998; 127-129: pp. 885-891.
[23] Willis, D.A., Xu, X.: Transport phenomena and droplet formation during pulsed laser interaction with thin films. Journal of Heat Transfer; 2000; 122: pp. 763-770.